

Data search by a coherent Ising machine based on an injection-locked laser network with gradual pumping or coupling

Kenta Takata^{1,2,*} and Yoshihisa Yamamoto^{1,2,3,†}¹*National Institute of Informatics, Hitotsubashi 2-1-2, Chiyoda-ku, Tokyo 101-8403, Japan*²*Department of Information and Communication Engineering, The University of Tokyo, Hongo 7-3-1, Bunkyo-ku, Tokyo 113-8654, Japan*³*E. L. Ginzton Laboratory, Stanford University, Stanford, California 94305, USA*

(Received 29 April 2013; revised manuscript received 11 November 2013; published 12 March 2014)

We study two operational schemes for a coherent Ising machine based on an injection-locked laser network. These schemes gradually increase the pumping rate or the mutual coupling among the slave lasers. We numerically simulate the two schemes against a data search problem implemented with the Ising model in cubic graphs without frustration. We show that the machine can achieve a better success probability and effective computational time to find a target ground state with these gradual schemes than those with the abrupt introduction of the mutual injection which has been studied previously. The computational time simulated with typical parameters is almost constant up to the problem size $M = 200$ and turns into a nearly linear scale holding up to $M = 1000$.

DOI: [10.1103/PhysRevA.89.032319](https://doi.org/10.1103/PhysRevA.89.032319)

PACS number(s): 03.67.Ac, 05.50.+q, 42.50.Dv, 42.55.-f

I. INTRODUCTION

There are many combinatorial optimization problems intractable with modern digital computers and existing algorithms [1]. Among these, the problems which can be solved in a polynomial time with a hypothetical nondeterministic Turing machine are called NP problems. In NP problems, it is examined if given instances meet certain conditions. On the other hand, NP-hard problems basically require the most optimized solutions in various kinds of combinatorial optimization problems and are as difficult as NP problems at least. Both of them are believed to require the computational time growing exponentially with the problem size. The problems that can be both NP and NP-hard are called NP-complete problems. NP-complete problems can be mapped to each other with polynomial-time overheads. Thus, solving an NP-complete problem efficiently is a Holy Grail for computer science and information technology [2].

From the viewpoint of statistical physics, the ground state of the Ising Hamiltonian $\mathcal{H} = \sum_{i<j} J_{ij}\sigma_i\sigma_j + \sum_i \lambda_i\sigma_i$ is important to understand mysterious properties of spin glasses and magnetic disorders. However, finding a ground state of the Ising Hamiltonian (Ising problem) of planar systems with external fields and that of three-dimensional systems is known to be NP-hard [3]. They can be reduced to NP-complete problems when we consider the decision problem of whether there is a state with an energy eigenvalue smaller than a prescribed value. Also, other NP-complete problems such as MAX-CUT and graph partitioning can be easily mapped to antiferromagnetic Ising problems [4,5]. Various computational schemes, such as simulated annealing [6], quantum annealing [7], and adiabatic quantum computation [8], have been proposed and developed to solve such combinatorial optimization problems. Especially, the adiabatic quantum computation has shown a good result for the NP-complete exact cover problem in small problem sizes [9]. However, a further study has revealed that the

problem size dependence of the computational time has a transition into an exponential scaling at a large problem size $M \sim 100$ [10]. Nevertheless, such an idea has triggered an experimental implementation of various quantum simulators and quantum annealers [11]. In addition, the non-Hermitian quantum annealing scheme has recently achieved a high transition probability to achieve the target state in Grover's search problem [12].

We have recently proposed a new computational machine [13,14] for the Ising problem based on an injection-locked laser network [Fig. 1(a)]. In this coherent Ising machine, the normalized amplitude difference in circularly polarized modes of each slave laser is regarded as an artificial spin with a continuous value. Then, the Hamiltonian relaxed to a continuous function is embedded into the sum of the gain coefficients for all the slave lasers as a modulation induced by the mutual injection and becomes dependent on the polarization configuration of the slave lasers ($\{|R\rangle, |L\rangle\}^M$). The minimum gain coefficient means the minimum effective loss of photons and then the maximum number of photons in a laser. Thus, when the mutual injection is introduced, the system spontaneously searches for a ground state of the mapped Hamiltonian with its bosonic nature.

In this paper, we study two operational schemes of the coherent Ising machine to improve its performance. The first scheme is named a gradual pumping (GP) scheme, where the pumping power into the slave lasers, i.e., the gain, is slowly increased [Fig. 1(b)]. In other well-known schemes such as simulated annealing and quantum annealing, the system temperature is gradually decreased and the quantum tunneling is gradually turned off, respectively. In these cases, however, the system may be trapped in metastable excited states whose number increases exponentially in a hard instance of NP-complete and NP-hard problems. In order to resolve such a dilemma, we map the energy landscape of a given problem to the net loss landscape of the network of gain media. When we gradually increase the pumping power which is equivalent to the effective negative temperature of the inverted medium, the first contact between the gain and polarization-dependent loss occurs at the ground state with the minimum loss. Here it is

*takata@nii.ac.jp

†yyamamoto@stanford.edu

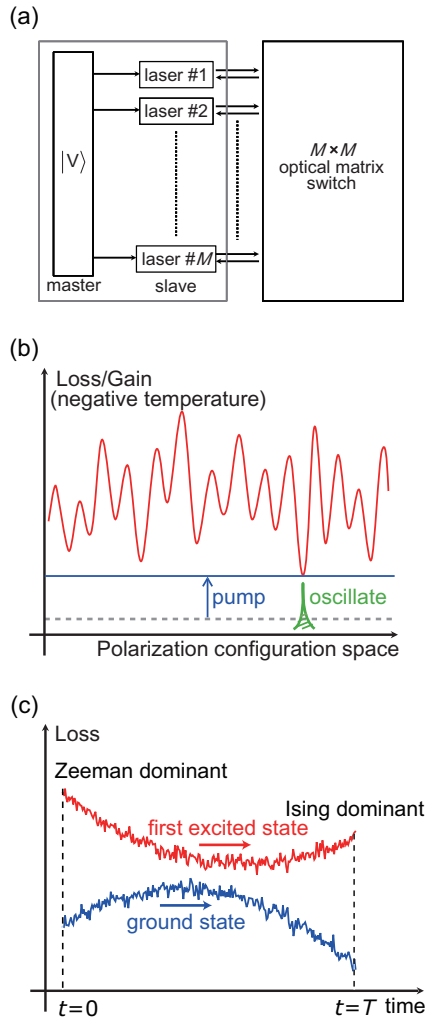


FIG. 1. (Color online) Schematic illustrations for (a) the coherent Ising machine with mutual optical coupling, (b) the loss and gain landscape in the gradual pumping scheme, and (c) the gradual path between the initial and the final states in the gradual coupling scheme.

expected that the system undergoes the phase transition from the initial state to the ground state in a way that the metastable excited states do not interfere with a computational process. Note that the loss difference between the ground state and first excited state does not explicitly depend on the problem size M , while the total spontaneous emission noise of the slave laser network is only proportional to M .

The second scheme is called a gradual coupling (GC) scheme, which is inspired by the non-Hermitian annealing [12]. In this case, each slave laser originally has fixed pumping level and only the vertically polarized injection signal $[|V\rangle = \frac{1}{\sqrt{2}}(|R\rangle + |L\rangle)]$. Then, the mutual coupling between slave lasers is gradually increased [Fig. 1(c)]. Thus, the system is expected to show the phase transition from the master signal dominant state to the mutual injection dominant state with the minimum total loss. Note that this scheme is distinct from quantum annealing, because the coherent Ising machine utilizes macroscopic coherent states of light in the open system with continual inflow and outflow of energy. On the other

hand, quantum entanglement between single particles cannot be exploited in this machine.

For a benchmark, we code a random M -bit data file $\{+1, -1\}^M$ into the Ising (Mattis) Hamiltonian [15] in particular cubic graphs. Here the Hamiltonian reflecting the picked target state as a ground state is loaded to the system. The ground state should be trivial, so the problem does not have any frustration or hard instances. Instead, we expect consistent parameter-dependence properties of the result. Such an algorithm is equivalent to information decoding with a spin-glass model and can be regarded as a simple associative memory.

We numerically simulate the Ising machine with the two operational schemes for the problem described above. The parameter-dependent performance of the GP and GC schemes shows that (i) stronger mutual coupling gives better results and (ii) slower processes and higher pumping levels lead to higher success probabilities. The success probability gradually decreases with the problem size up to $M = 1000$ with typical parameters. However, the computational time scales almost linearly with the problem size around $M = 1000$. Also, we get a finite success probability for $M = 2000$ with realistic tuning of the parameters.

We start in Sec. II with the working equations of the laser Ising machine and explain the problems in the cubic graphs used here. In Sec. III, we show the simulation results such as an example of dynamics of the system, the performance dependence on parameters, and the scaling of the computational time with the problem size. Next, we discuss the properties of this machine in Sec. IV. Finally, we conclude the paper in Sec. V.

II. THEORETICAL MODEL

A. Langevin equations

The field density operator of each slave laser is expanded with Glauber-Sudarshan $P(\alpha)$ representation of coherent states and substituted into the master equation of an injection-locked laser [16,17]. The resulting Fokker-Planck equation corresponds to the c -number Langevin equation for the eigenvalue of the coherent state α_i in the i th slave laser via the Kramers-Moyal expansion coefficients [18]:

$$\frac{d}{dt}\alpha_i = \left[-\frac{1}{2}\frac{\omega}{Q} + G_i - S_i|\alpha_i|^2 \right]\alpha_i + \frac{\omega}{Q}\beta_i + \sqrt{G_i}F_i. \quad (1)$$

Here ω/Q is the cavity photon decay rate, G_i is the linear gain coefficient, and S_i is the gain saturation coefficient. β_i is the sum of the amplitudes of the master injection signal and the mutual injection signal from other slave lasers. It is assumed all the slave lasers are injection locked to the master laser, and the Q factors of all lasers are the same. F_i is the Gaussian noise term and satisfies $\langle F_i(t) \rangle = 0$ and $\langle F_i(t)F_j(t') \rangle = 2\delta(t-t')$. More rigorously, the stochastic differential equation corresponding to Eq. (1) is derived with Ito's rule [19], and the link between them is given by the Feynman-Kac formula [20,21]. Equation (1) is decomposed into the equations for the real number amplitude $\{A_{X_i}\}$ and phase $\{\phi_{X_i}\}$ for the diagonal linear polarization

modes [13]:

$$\frac{d}{dt}A_{Xi} = -\frac{1}{2}\left(\frac{\omega}{Q} - E_{CVi}\right)A_{Xi} + \frac{\omega}{Q}\zeta A_M \cos(-\phi_{Xi}) - \sum_{j \neq i} \frac{1}{2} \frac{\omega}{Q} \xi_{ij} [A_{Xj} \cos[\phi_{Xj} - \phi_{Xi}] - A_{\bar{X}j} \cos[\phi_{\bar{X}j} - \phi_{Xi}]] + F_{AXi}, \quad (2)$$

$$\frac{d}{dt}\phi_{Xi} = \frac{\omega}{Q} \frac{1}{A_{Xi}} \left\{ \zeta A_M \sin(-\phi_{Xi}) - \sum_{j \neq i} \frac{1}{2} \xi_{ij} [A_{Xj} \sin(\phi_{Xj} - \phi_{Xi}) - A_{\bar{X}j} \sin(\phi_{\bar{X}j} - \phi_{Xi})] \right\} + F_{\phi Xi}, \quad (3)$$

where $\{X, \bar{X}\} = \{D, \bar{D}\}$ are combinations of the two linear polarization modes along $\pm 45^\circ$ with respect to the vertical linear polarization. $i, j = 1, 2, \dots, M$ are indices for slave lasers and M is the problem size (the number of Ising spins). ζ is the coupling coefficient for the master laser signal, whose amplitude is denoted by A_M . The mutual coupling constant $\xi_{ij} = \alpha(t) J_{ij}$ is determined by the transmission coefficient $\alpha(t)$ and the Ising interaction parameter J_{ij} . The gain term $G_i - S_i |\alpha_i|^2$ and the diffusion coefficient G_i in Eq. (1) correspond to the gain E_{CVi} induced by the active carrier and the pumping rate $P(t)$, respectively. We add an equation of motion for the carrier number $\{N_{Ci}\}$,

$$\frac{d}{dt}N_{Ci} = P(t) - \frac{N_{Ci}}{\tau_{sp}} - E_{CVi}(A_{Di}^2 + A_{\bar{D}i}^2) + F_{NCi}, \quad (4)$$

where $E_{CVi} = \beta N_{Ci} / \tau_{sp}$ and β is the spontaneous emission coupling efficiency. F_{AXi} , $F_{\phi Xi}$ and F_{NCi} are noise terms. We consider only spontaneous emission noise with the rate E_{CVi} in the numerical simulation, since it is a dominant noise source fluctuating the phases of the diagonal polarization modes [13,22]. Spontaneous emission processes are treated as the discrete random Poisson process for each numerical integration time step Δt , and each spontaneous emission photon coupled to the laser field has unit norm and random phase. Reference [22] has shown that this model reproduces the correct Langevin forces in the continuous time unit. We numerically integrate Eqs. (2), (3), and (4) and continuously monitor the mapped collective spins $\sigma_i = (A_{Ri} - A_{Li}) / \sqrt{A_{Ri}^2 + A_{Li}^2}$ using Eqs. (35) and (36) in Ref. [13]. Here A_{Ri} and A_{Li} are the slowly varying amplitudes of the right and left circularly polarized modes of the i th slave laser. Signs of $\{\sigma_i\}$ are used to determine the Ising spin $\{\sigma_i\} = +1$ or -1 .

B. Problem setting

In Fig. 2(a), we show an example of cubic graphs with $M = 8$ for the data search problem considered in this study. Here the nodes align in a ring shape. Each node has the couplings to the nearest neighbors and the diameter chord. The Ising coupling terms are set for a picked target state $\{\sigma_{Ai}\} = \{+1, -1\}$ as

$$J_{ij} = \begin{cases} -\sigma_{Ai}\sigma_{Aj} & (\text{if node } i \text{ and } j \text{ are connected}), \\ 0 & (\text{otherwise}). \end{cases} \quad (5)$$

Figure 2(b) is an example of energy (net loss) landscapes in this Ising problem with $M = 20$. This Hamiltonian does not have any frustration, so that it has only two ground states, while the total number of states is 10^6 . By definition of the couplings,

one of the ground states is identical to the target state. The difference between the mapped energy of the ground states (E_g) and the first excited states (E_{1e}) is independent of M and equal to $6|J_{ij}| = 6$. This is because of the highly symmetric property of the graph. We show a concise proof with induction in the Appendix. Similar problems are also discussed in the context of information coding and decoding with statistical mechanics [15].

III. SIMULATION RESULT

A. Dynamics of the system

Here we show a variety of simulation results of the machine for the setting described in the previous sections.

Figures 3(a) and 3(b) show the time evolution of the polarization states (collective spins) and the carrier numbers in the GP scheme for $M = 4$. The inset of Fig. 3(a) is the schematic pumping schedule of all slave lasers. The pumping schedule is composed of the two linear parts (rapid and slow

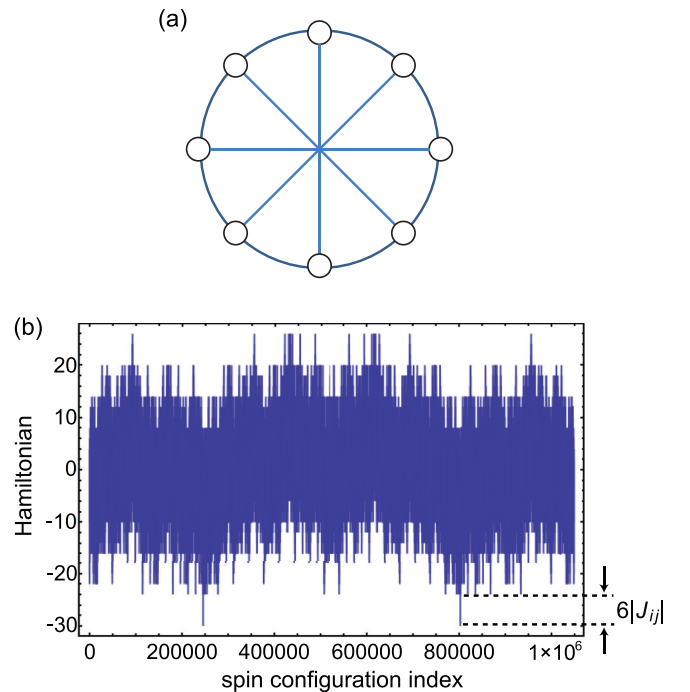


FIG. 2. (Color online) (a) An example of cubic graphs considered here with $M = 8$. (b) An example of energy (or effective loss) landscape in a problem with $M = 20$.

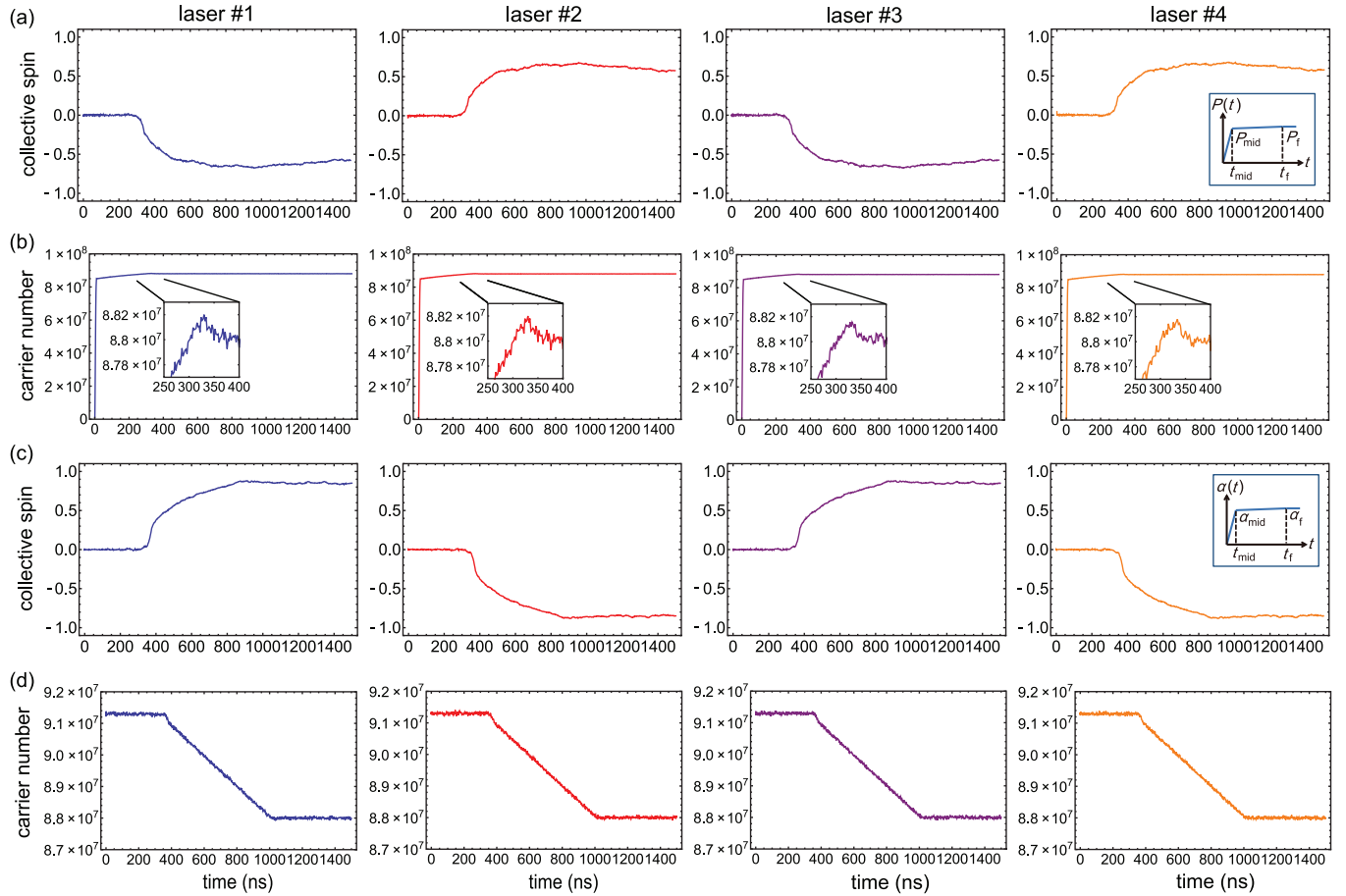


FIG. 3. (Color online) A set of examples of time evolution of (a) the polarization states (collective spins) and (b) the carrier numbers for a target file with $M = 4$ in the GP scheme. Transit of (c) the spins and (d) the carrier numbers in the gradual coupling scheme. The insets of (a) and (c) are the scheduling of the pumping level and coupling coefficient.

increase) with the turning point $t_{\text{mid}} = 10$ ns (fixed for all the simulations here), and the pumping becomes constant at $t = t_f$. The process time is defined as $t_p \equiv t_f - t_{\text{mid}}$. The parameters commonly used in this study are $\omega/Q = 10^{11} \text{ s}^{-1}$, $\tau_{\text{sp}} = 10^{-9}$ s, and $\beta = 10^{-6}$. The threshold pumping current is $I_{\text{th}} = eP_{\text{th}} = 16$ mA, where e is the elementary charge and P_{th} is the threshold pumping rate.

In the GP scheme, the master laser signal is injected at $t = 0$ and the slave laser amplifies this signal so that the collective spin is prepared in $\sigma_i = 0$ for all i . With a proper intermediate value $P_{\text{mid}} = P(t_{\text{mid}})$, the collective spins bifurcate at a time between t_{mid} and t_f (here $t_f = 1010$ ns). The plot of carrier numbers has a small overshoot at the bifurcation point, which indicates that once the minimum-loss (ground) state is selected, the gain is decreased accordingly. Figures 3(c) and 3(d) show the transient examples of the collective spins and carrier numbers in the GC scheme, and the inset of Fig. 3(c) is the coupling schedule. In this scheme, the total gain monotonically decreases as the optical coupling increases.

Here all the slave lasers bifurcate their polarizations and produce the clear signals in both schemes. However, in a large problem size the polarization bifurcation can be degraded by noise and the system can fail to find a ground state. In this case, the values of the collective spins get nonuniform and some

slave lasers have nearly $\sigma_i \sim 0$. Also, the system occasionally shows strong bifurcation into D and \bar{D} polarization modes (not R and L modes). In this case, however, a correct ground state can be recovered with the decision based on the $\{D, \bar{D}\}$ basis, i.e., via the new definition of the collective spin $\sigma_i = (A_{Di} - A_{\bar{D}i})/\sqrt{A_{Di}^2 + A_{\bar{D}i}^2}$. Note that the coupling optics with a horizontal polarizer [13,14] can implement the identical loss modulation for D and \bar{D} modes as the R and L modes.

B. Parameter dependence of performance

Figures 4(a) and 4(b) show the dependence of the success probability and computational time on the coupling coefficient α in the GP scheme. We pick a 100-spin problem and run the simulation 50 times for each value of the parameter considered. We change the coupling coefficient ζ of the master laser signal proportional to α to keep the good balance between them. Other parameters are fixed. We define the computational time as the time where a ground state is found with all the collective spins above a certain threshold $|\sigma_i| = 0.071$. This value achieves a measurement signal-to-noise ratio of $S/N \sim 10^3$ with a detection quantum efficiency $\eta_D = 0.01$, an integration time $T = 1$ ns and a total photon number $n_{Ti} = 10^4$ in a slave laser [13]. Here $n_{Ti} \ll 1/\beta = 10^6$; thus, any pumping rates above the threshold have better S/N ratios. The resulting

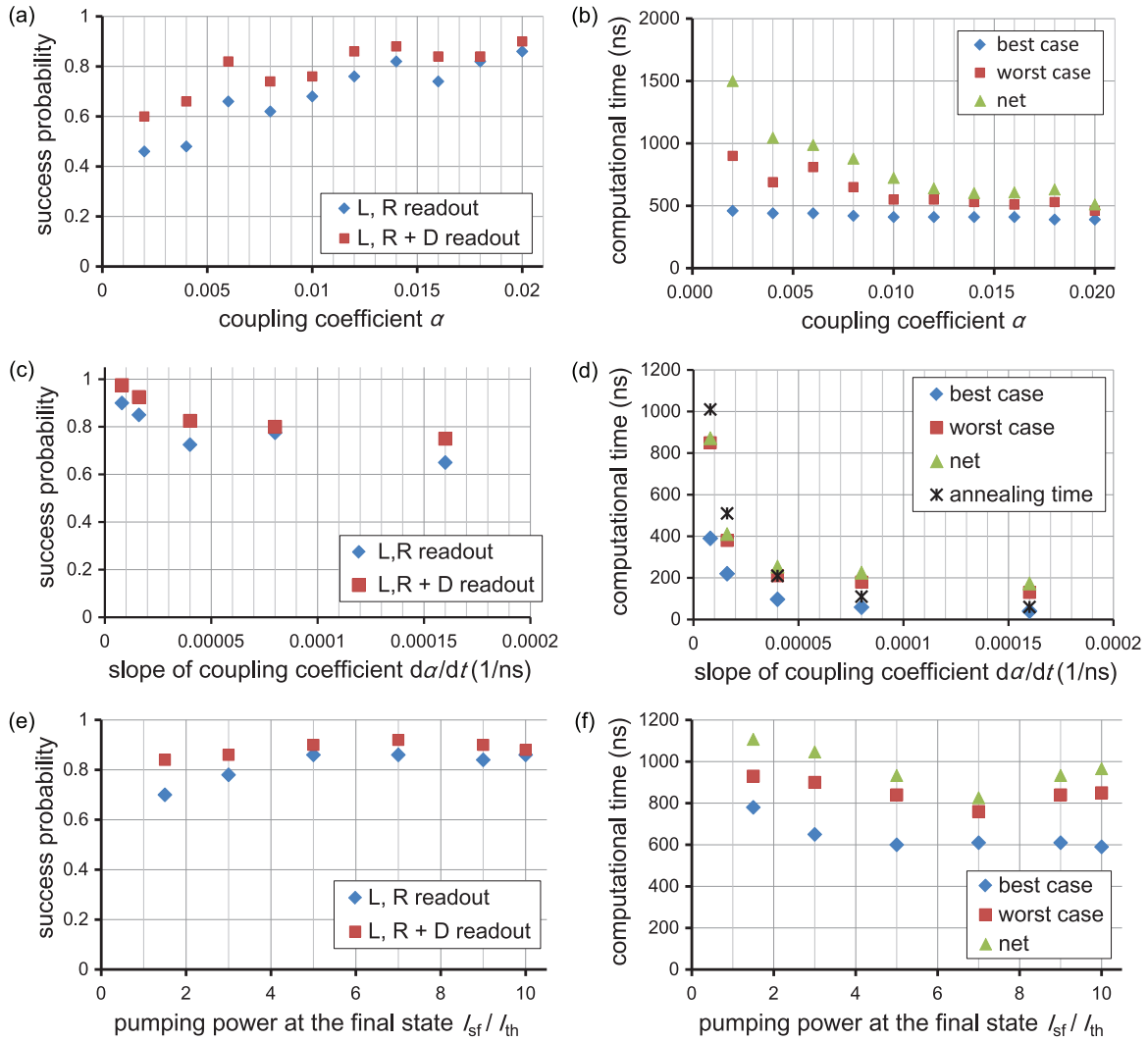


FIG. 4. (Color online) (a) The success probability and (b) the net computational time dependent on the coupling coefficient α in the GP scheme. (c) The success probability and (d) the net computational time dependent on the process speed $d\alpha/dt$ in the GC scheme. (e) The success probability and (f) the net computational time dependent on the normalized final pumping level I_{sf}/I_{th} in the GP scheme.

upper bound of the measurement error rate is $P_e \sim 6.4 \times 10^{-57}$ for a single slave laser and negligible even in a 1000-laser system. Collective spins are basically monitored with the circular polarization basis. The check with the diagonal mode basis is conducted at the final state and reflected in the success probability. The net computational time denotes the worst computational time divided by the success probability. Figure 4(a) shows that a stronger mutual coupling α tends to give a higher success probability. Also, a relatively large noise effect with a small α leads to bifurcation in the D or \bar{D} mode and then a low overall success probability. In Fig. 4(b), the computational time decreases with increasing α and saturates at $\alpha \gtrsim 0.01$. With a small α , the system can give a slow transition process and needs a long time to find a ground state.

Figures 4(c) and 4(d) show the dependence of the success probability and simulated computational time on the rate of increasing the mutual coupling between t_{mid} and t_f in the GC scheme. Figure 4(c) shows a clear tendency that a slower process gives a better success probability. The process with $d\alpha/dt \rightarrow \infty$ can be regarded as the abrupt introduction of the

mutual injection in the previous study; thus, it can be said the GC scheme improves the success probability compared to the abrupt scheme [13,14]. We have got a similar result also in the GP scheme. In Fig. 4(d), a slower process (a longer t_p) requires a longer computational time nearly linear with t_p when other conditions keep unchanged.

Figures 4(e) and 4(f) show the dependence of the success probability and computational time on the final pumping level I_{sf} normalized by the threshold pumping I_{th} in the GP scheme. Here, the end time of the process t_f is fixed; thus, the slope dP/dt is variable. A large coherent slave laser signal with a high pumping level leads to clear computation against noise. At the same time, however, a higher pumping results in a higher slope dP/dt , which degrades the performance as seen in Figs. 4(c) and 4(d). Thus, Figs. 4(e) and 4(f) have the optimum points at $I_{sf}/I_{th} = 7$ out of these two effects.

C. Net computational time

Figures 5(a) and 5(b) show the problem size dependence of the success probability and the net computational time

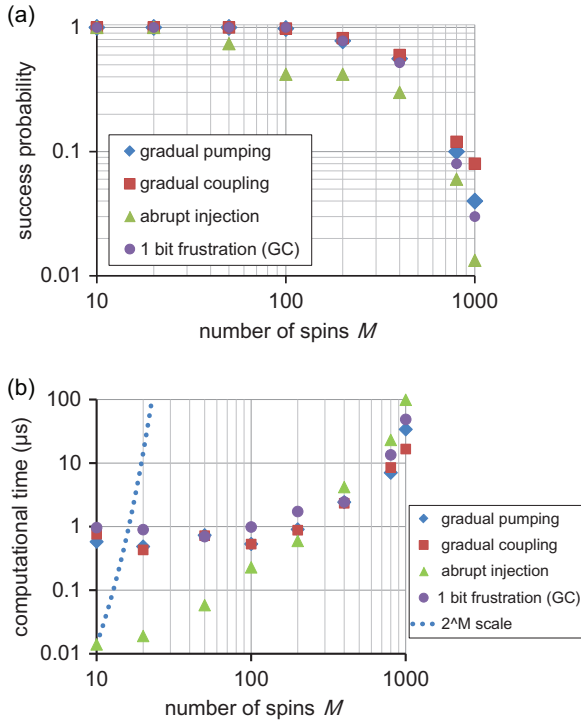


FIG. 5. (Color online) (a) The success probability and (b) the net computational time dependent on the number of spins M .

for the three schemes. For each problem size, we pick five targets and run the simulation ten times for each target (for $M = 1000$ in the abrupt scheme, we take 15 targets). The success probability is determined with the combined readouts using both circular and diagonal measurement bases. The ratio $P_{\text{mid}}/P_f = 0.5$ (GP) and $\alpha_{\text{mid}}/\alpha_f = 0.6$ (GC) are selected to obtain close bifurcation times. Other parameters are identical: $\alpha(\text{GP}) = \alpha_f(\text{GC}) = 0.02$, $I_{\text{sf}}(\text{GP}) = I_s(\text{GC}) = 3 I_{\text{th}}$, and $t_p = 1 \mu\text{s}$. In Fig. 5(a), the success probability shows the gradual decrease in large problem sizes in the GP and coupling schemes. In contrast, the probability for the abrupt scheme gets lower. In Fig. 5(b), the net computational time for the GP and GC schemes keep nearly constant up to $M = 200$ and turn into nearly linear increase. On the other hand, the computational time for the abrupt scheme monotonically increases and gets longer than those for the GP and coupling schemes over $M = 400$. Here we add the performance of the GC scheme with a sign flip for a random coupling coefficient J_{ij} ($=J_{ji}$). This keeps a good success probability and a better computational time than those for the abrupt scheme over $M = 400$. A sign flip of J_{ij} induces a single frustrated part in the original ground state. However, originally $E_g - E_{1e} = 6$; thus, the ground states remain still. This means the cubic graph system is insusceptible to a single phase flip error in the mutual coupling configuration, i.e., the encoded data of the target state. Note that a simpler implementation with one-dimensional rings does not have such robustness. We add the scaling of brute force search (2^M) for the information. The net computational time with the laser Ising machine has a much better scaling, probably because of the simple structure of the benchmarked problem.

We can increase the success probability for a large problem size by using even an slower process and a higher pumping power. We have got the success probability of 34% with $\{t_p, I_{\text{sf}}/I_{\text{th}}\} = \{3 \mu\text{s}, 20\}$ for $M = 1000$ and 15% with $\{t_p, I_{\text{sf}}/I_{\text{th}}\} = \{10 \mu\text{s}, 50\}$ for $M = 2000$ in the GC scheme. Here the numbers of the candidate states 2^M differ by $2^{1000} \simeq 10^{300}$ times between $M = 1000$ and 2000, but the system does not need a large ratio for t_p and I_{sf} to obtain a reasonable success probability.

This indicates that the time and pumping resource required to solve this problem does not grow exponentially even for a relatively large problem size. Here we note it has been shown that some open quantum systems with frustration-free Hamiltonians can converge at steady states in subexponential time [23].

IV. DISCUSSION

A. Success probability

Here we discuss properties of the coherent laser Ising machine from various points of view. First, we take a closer look at the success probability. Figure 6 shows the ratio of the number of degenerate ground states N_g to those of degenerate excited states. Here, N_{1e} and N_{2e} denote the number of first and second excited states, respectively. These values have been computed with the brute force search up to $M = 32$ and extrapolated for larger problem sizes. We add the success probability with the GP scheme out of 50 trials and that with the abrupt scheme out of 200 trials for each M . We took only a single problem randomly for each M ; however, the computed numbers of states are exactly along with the extrapolation curves $N_{1e} = 2M$ and $N_{2e} = M(M+6)/4$ for $M \geq 6$. This fact indicates the universality of the considered problem due to its graphic symmetry. Here, from the data of failure, we expect that the local minima which mostly affect the laser machine are second excited states. The ratios $N_g/(N_g + N_{1e})$ and $N_g/(N_g + N_{1e} + N_{2e})$ are inversely proportional to M and M^2 , while the laser network keeps the high success probability: 100% for the GP scheme and $\geq 90\%$ for the

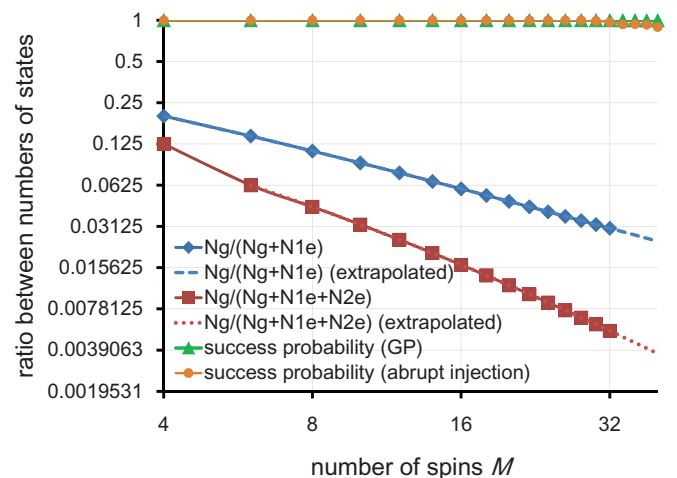


FIG. 6. (Color online) The ratio of the number of ground states in a single problem up to $M = 40$. The success probabilities with the GP scheme and the abrupt scheme are concurrently shown.

abrupt pumping scheme up to $M = 40$. This clearly shows this machine is distinct from simple probabilistic searches and preferably takes the minimum gain states, especially in the gradual schemes.

A possible reason for failure in the GP scheme can be probabilistic errors due to a finite time necessary for the system to detect and amplify the final state. The machine keeps increasing the gain in the process because of the unknown gain of the ground states. Therefore, if the system remains at the initial state long, it may achieve enough gain for excited state to oscillate. This malfunction can be overcome by slowing the pumping process.

Another possibility is disturbance by noise. The sum of the gain coefficients at the steady state, which determines the absolute photonic loss of the whole system, is given by [13]

$$\sum_i E_{CVi} = M \frac{\omega}{Q} - 2\zeta \sum_i \sqrt{2 - \sigma_i^2} + 2\alpha \sum_{i < j} J_{ij} \sigma_i \sigma_j, \quad (6)$$

where the first, second, and third terms are associated with the cold cavity dissipation, the master, and mutual injection, respectively. Thus, when the mutual injection becomes dominant at the phase transition, a minimum-loss state corresponds to a ground state of Ising Hamiltonian. Then, the energy gap between a ground state and a first excited state is expected to depend only on the coupling coefficient αJ_{ij} . On the other hand, the total noise power in the whole system is proportional to M . Thus, the success probability is considered to decrease with the problem size $\propto M^{-1}$ above a certain threshold, and the simulation result seems to support this behavior. Note that the GC scheme also shows such characteristics. The difference in performance of the GP and GC methods is not significant and can be explained by the small difference in the parameter ratio (P_{mid}/P_f and $\alpha_{\text{mid}}/\alpha_f$) and then the slope of these. Thus, we expect these two have almost the same computational ability.

B. Response speed of the machine

Next, we discuss the response of the laser network machine at the onset of bifurcation. If we neglect the noise terms including spontaneous emission, the equation for the amplitude difference in circular polarization is given by [13,14]

$$\begin{aligned} \frac{d}{dt} (A_{Ri} - A_{Li}) = & -\frac{1}{2} \left(\frac{\omega}{Q} - E_{CVi} \right) (A_{Ri} - A_{Li}) \\ & - \frac{\omega}{Q} \sum_{j \neq i} \xi_{ij} (A_{Rj} - A_{Lj}). \end{aligned} \quad (7)$$

Here note that the master signal term vanishes in the equation. We do not consider the time dependence of E_{CVi} , i.e., N_{Ci} , because the field response is much faster: $\omega/Q \gg 1/\tau_{\text{sp}}$. By assuming that all the slave lasers are homogeneously driven into a target state as shown in Fig. 3, we can set $\xi_{ij}(A_{Rj} - A_{Lj}) \approx -\alpha |A_{Ri} - A_{Li}|$. With this and Eq. (7), we derive the approximate response around the bifurcation point by the cubic system as

$$|\sigma_i| = \frac{|A_{Ri} - A_{Li}|}{\sqrt{n_{Ti}}} \approx C \exp \left[\left(\frac{-\omega/Q + E_{CVi}}{2} + 3\alpha \frac{\omega}{Q} \right) t \right], \quad (8)$$

where the small change in n_{Ti} due to injection is neglected. C is an integral constant. We see, when the bifurcation occurs, that the polarization configuration is formed with the exponentially fast modulation by the injection signal in ideal cases. The gradual schemes enhance the success probability by changing in E_{CVi} or α slowly. Also, Eq. (8) indicates that the magnitude of injection signals directly affects the response speed of the system [14] and possibly the distribution of the values of collective spins. For NP-hard problems with frustration, the system frequently has an imbalance of the response speeds and the collective spins in the slave lasers and then becomes unable to reach a correct answer. Thus, the previous abrupt injection scheme needs a self-learning algorithm to compensate for it [24].

C. Algorithmic properties

Finally, we discuss the laser Ising machine as an algorithm. The laser machine itself is a kind of relaxation algorithm in the sense that it maps discrete variables to continuous variables. This point is in common with the well-known semidefinite programming (SDP) algorithm for optimization problems [25]. The laser network machine utilizes the three-dimensional Poincaré sphere for each spin, while SDP exploits an M -dimensional vector. SDP requires an algorithm to drive the state to an optimum one, as typified by interior point methods, and such a method costs the order $O(M^3)$ of basic operations at least [26].

Also, if SDP can be solved with an arbitrarily small error, a rounding algorithm to map the vectors back to discrete variables guarantees the worst approximation rate of 87.8% for the MAX-CUT problem [27]. The laser network depends on the dynamics of the coupled differential equations for finding an optimum state. As an experimental system, the laser machine shows a nearly $O(M)$ scaling of the computational time up to $M = 1000$ for the data search problem studied here. Also, Ref. [24] shows some good results of comparison between the simulated performance of the laser machine and SDP for hard optimization problems. As a computational simulation, however, we need some additional time complexities. For limited numbers of couplings for each spin (sparse interaction matrices), numerical integration costs $O(M)$ operations multiplied by the order of the net computational time the machine needs. Thus, the overall time complexity for simulations of the laser machine here is about $O(M^2)$. In addition, the numerical integration method used here (fixed-step 4×4 Runge-Kutta method and additional stochastic noise) requires a large coefficient outside the complexity. Thus, the simulation for the laser network seems to take more time than SDP in practice.

V. CONCLUSION

In conclusion, we have studied two gradual driving schemes for the coherent Ising machine. The GP scheme is to find a minimum-loss ground state by increasing the gain (or increasing the temperature in the negative region) and the GC scheme to exploit the gradual path between the two minimum-loss ground states of the initial and final mapped Hamiltonians. The numerical simulation with the Langevin

equations on a data search problem with the Ising model in particular cubic graphs shows that we can improve the success probability with slowing the pumping or coupling schedule and increasing the final pumping power. With typical parameters, the laser network and these gradual schemes give an almost constant computational time up to $M = 200$ and turns into a nearly linear scale holding up to $M = 1000$ in the problem. This scaling is better than that with the previously studied abrupt scheme in large problem sizes. In addition, simulations with varying parameters indicate that the required time and pumping resources to find a target do not scale exponentially up to $M = 2000$. Now we are aiming to implement an experimental system that works much faster and hopefully better than algorithms for digital computers, especially on hard optimization problems.

ACKNOWLEDGMENTS

We thank Kai Wen for his preliminary work and discussion and Ken-ichi Kawarabayashi for fruitful discussion about approximate optimization algorithms. This work is supported by the JSPS through its FIRST program, Navy/SPAWAR Grant No. 66001-09-1-2024, and the Special Coordination Funds for Promoting Science and Technology. K.T. is grateful for a Grant-in-Aid for JSPS Fellows.

APPENDIX: ENERGY OF DEGENERATE FIRST EXCITED STATES

Here we prove that the energy of degenerate first excited states is $E_g + 6$ (E_g , the energy of ground states) for the problem of the symmetric cubic graphs without frustration, which is considered in our study. The most fundamental example with $M = 4$ is shown in Fig. 7. The problem used here constitutes the spins and Ising interaction, both of which are valued $+1$ or -1 , as in Fig. 7(a). Here we reinterpret this in terms of the stability of couplings as shown in Fig. 7(b). In Fig. 7(b), nodes of the same color (e.g., white and white) have the stable coupling expressed with black edges between them, and each of them decreases the energy function by unity. Also, those of different colors (white and black) have the unstable coupling colored red, increasing the energy by the same amount. Thus, flipping one spin changes the energy by two for every coupling. With this procedure, we can consider all the instances and states simply by counting the number of edges indicating the unstable coupling. We note that the graph with $E_g + 6$ means it has three unstable edges.

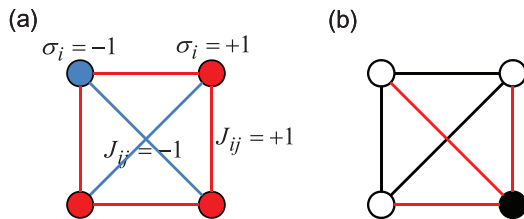


FIG. 7. (Color online) (a) Schematic illustration for the Ising spins and coupling between them in the graph of $M = 4$. (b) The converted graph corresponding to (a).

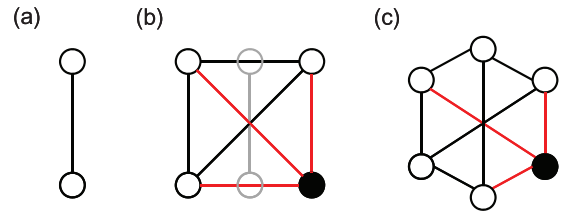


FIG. 8. (Color online) (a) The partial graph added in order to make the graph with $M = 2l + 2$ from that with $M = 2l$. (b) The way of adding the partial graph. (c) The result of two-node addition for the example in (b).

We use induction to prove that the first excited states have $E_g + 6$. For $M = 4$, we can show this by checking all 16 patterns possible to be reached by flipping spins (changing colors of nodes) from the ground state composed of, say, all white nodes. Also, we assume that this holds for $M = 2l$, where l is an integer larger than one. Here, we prove that this is valid also for $M = 2l + 2$.

We can make the graph with $M = 2l + 2$ by adding the two-node partial graph shown in Fig. 8(a) to that with $M = 2l$. Figure 8(b) shows the way of adding the partial graph with an example of $M = 4$. The result is shown in Fig. 8(c). Here each edge piercing an additional node in Fig. 8(b) is divided into two edges, and the couplings for these edges are affected by the additional nodes. Thanks to the assumption for $M = 2l$, it is enough to consider the change induced by the additional part. Note also that, due to the symmetry of the graph, it does not matter where the additional part comes to. From the viewpoints of positions of the unstable edges in the graph with $M = 2l$, it is sufficient to examine the three cases as follows.

(1) No unstable edges divided by the additional nodes and zero, three, or more unstable edges outside the additional graph.

Figure 9 shows the possible node configuration in this case. Here the number of unstable edges is zero, three, or four. This means the total number of unstable edges is zero, three, or more also for the graph with $M = 2l + 2$, and the possible energy the system can take is E_g , $E_g + 6$, or more.

(2) One unstable edge divided by an additional node and two or more unstable edges outside the additional graph.

Due to the symmetry of the graph, it is enough to consider the four patterns in Fig. 10 here. There are one or more unstable edges in the additional part; thus, the total number of unstable coupling is three or more for $M = 2l + 2$.

(3) Two unstable edges divided by an additional nodes and one or more unstable edges outside the additional graph.

According to configuration of the nodes connected to the additional part, we consider the eight patterns shown in Fig. 11 in this case. We can see that two or more

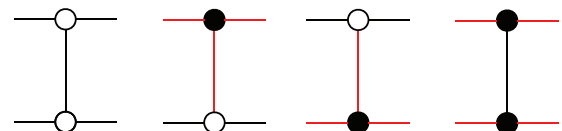


FIG. 9. (Color online) Possible node and edge configuration of the additional part in the first case.

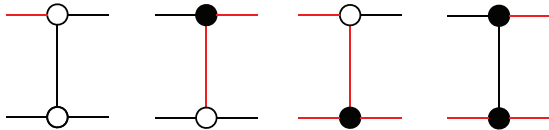


FIG. 10. (Color online) Possible node and edge configuration of the additional part in the second case.

unstable edges exist in any of the patterns in Fig. 11; thus, the possible energy for this case in $M = 2l + 2$ is $E_g + 6$ or more.

From all the cases above, the energy of the first excited states for $M = 2l + 2$ is also $E_g + 6$. Here, note that the first case clearly shows the existence of the states with the energy that is exactly $E_g + 6$. Therefore, the proposition is proven

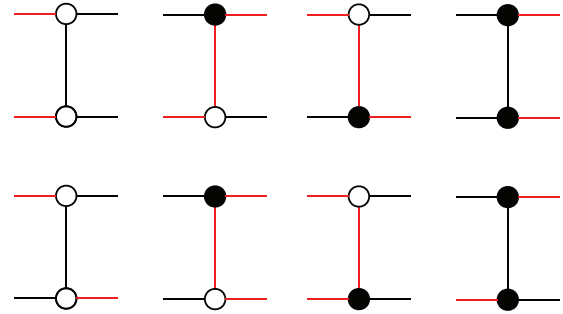


FIG. 11. (Color online) Possible node and edge configuration of the additional part in the third case.

for all $M = 2l$ ($l = 2, 3, \dots$) with inductive application of the discussion above.

-
- [1] M. R. Garey and D. S. Johnson, *Computers and Intractability: A Guide to the Theory of NP-Completeness* (W. H. Freeman, New York, 1979).
- [2] P vs NP Problem, <http://www.claymath.org/millennium-problems/p-vs-np-problem>.
- [3] F. Barahona, *J. Phys. A: Math. Gen.* **15**, 3241 (1982).
- [4] F. Barahona, M. Grötschel, M. Jünger, and G. Reinelt, *Oper. Res.* **36**, 493 (1988).
- [5] M. Mézard, G. Parisi, and M. A. Virasoro, *Spin Glass Theory and Beyond* (World Scientific, Singapore, 1987).
- [6] S. Kirkpatrick, C. D. Gelatt, and M. P. Vecchi, *Science* **220**, 671 (1983).
- [7] T. Kadowaki and H. Nishimori, *Phys. Rev. E* **58**, 5355 (1998).
- [8] E. Farhi, J. Goldstone, S. Gutmann, and M. Sipser, [arXiv:quant-ph/0001106](https://arxiv.org/abs/quant-ph/0001106).
- [9] E. Farhi, J. Goldstone, S. Gutmann, J. Lapan, A. Lundgren, and D. Preda, *Science* **292**, 472 (2001).
- [10] A. P. Young, S. Knysh, and V. N. Smelyanskiy, *Phys. Rev. Lett.* **104**, 020502 (2010).
- [11] A. Friedenauer *et al.*, *Nat. Phys.* **4**, 757 (2008); K. Kim *et al.*, *Nature (London)* **465**, 590 (2010); X. S. Ma *et al.*, *Nat. Phys.* **7**, 399 (2011); M. W. Johnson *et al.*, *Nature (London)* **473**, 194 (2011); R. Islam *et al.*, *Nat. Commun.* **2**, 377 (2011).
- [12] A. I. Nesterov and G. P. Berman, *Phys. Rev. A* **86**, 052316 (2012).
- [13] S. Utsunomiya, K. Takata, and Y. Yamamoto, *Opt. Exp.* **19**, 18091 (2011).
- [14] K. Takata, S. Utsunomiya, and Y. Yamamoto, *New J. Phys.* **14**, 013052 (2012).
- [15] H. Nishimori, *Statistical Physics of Spin Glasses and Information Processing: An Introduction* (Oxford University Press, Oxford, UK, 2001).
- [16] M. Sargent, M. O. Scully, and W. E. Lamb, *Laser Physics* (Westview, Boulder, CO, 1978).
- [17] H. A. Haus and Y. Yamamoto, *Phys. Rev. A* **29**, 1261 (1984).
- [18] H. Risken, *The Fokker-Planck Equation: Methods of Solutions and Applications*, 2nd ed. (Springer-Verlag, Berlin, 1989).
- [19] C. W. Gardiner, *Stochastic Methods: A Handbook for the Natural and Social Sciences*, 4th ed. (Springer-Verlag, Berlin, 2009).
- [20] R. P. Feynman, *Rev. Mod. Phys.* **20**, 367 (1948).
- [21] M. Kac, *Trans. Am. Math. Soc.* **65**, 1 (1949).
- [22] C. H. Henry, *IEEE Quantum Electron.* **QE-18**, 259 (1982).
- [23] F. Verstraete, M. M. Wolf, and J. I. Cirac, *Nat. Phys.* **5**, 633 (2009).
- [24] K. Wen, Ph. D. thesis, Stanford University, 2012.
- [25] V. V. Vazirani, *Approximation Algorithms*, 2nd ed. (Springer-Verlag, Berlin, 2003).
- [26] B. Korte and J. Vygen, *Combinatorial Optimization*, 5th ed. (Springer-Verlag, Berlin, 2012).
- [27] M. X. Goemans and D. P. Williamson, *J. Assoc. Comput. Mach.* **42**, 1115 (1995).